THE ASTROPHYSICAL JOURNAL, 319:709–722, 1987 August 15

HIGH-REDSHIFT QSO ABSORBING CLOUDS AND THE BACKGROUND IONIZING SOURCE

R. F. CARSWELL[1]
Institute of Astronomy, Cambridge

J. K. WEBB
Institute of Astronomy, Cambridge; and Sterrewacht Leiden

AND

J. A. BALDWIN AND B. ATWOOD
Cerro Tololo Interamerican Observatory, National Optical Astronomy Observatories[2]
Received 1986 June 23; accepted 1987 February 3

ABSTRACT

Echelle spectra of the high-redshift QSO PKS 2000−330 have been analyzed to provide redshifts, H I column densities, and velocity dispersions of Lyman line absorbing systems in the redshift range $3.02 < z < 3.75$. The H I column density distribution function may not be well approximated by a power law, as had been suggested in earlier work, but instead shows a possible flattening towards lower values of the H I column density. For simple uniform cloud models, the redshift evolution of this distribution could in principle be used to infer the redshift dependence of the density of the gas within the clouds.

It is found that the source of ionization of these clouds cannot be the integrated light from background quasars, *if* the quasar density distribution cuts off between $z \approx 2$ and $z \approx 4$ as is commonly thought.

Subject headings: galaxies: intergalactic medium — quasars

I. INTRODUCTION

The lines of sight from us to the most distant quasars are populated by gas clouds which can be recognized only by the Lyman absorption lines which they superpose on the spectrum of the background quasar. Mixed in with these are lesser numbers of absorbing systems which show lines of heavier elements as well as those of hydrogen, and which are believed to be identified with the disks or halos of intervening galaxies (e.g., review by Weymann, Carswell, and Smith 1981). It is the first, Lyman line only, population which we examine further here.

Since the work of Peterson (1978) it has been known that there is a strong redshift dependence in the numbers of these clouds. Continuing intermediate resolution (1–2 Å) spectroscopy of a large sample of quasars has provided unambiguous evidence that there is genuine evolution in the comoving density of the clouds when they are counted down to some limiting absorption-line rest equivalent width (Murdoch *et al.* 1986). However, intermediate-resolution observations are not adequate to resolve the majority of these absorption lines, many of which are blended. Thus they provide little information about the individual cloud column densities and velocity dispersions associated with the observed equivalent widths.

In fact, there is very little information in general on the nature of these absorbing clouds. It is supposed they are ionized by a background radiation source, with the integrated light of all quasars being a good candidate (Chaffee *et al.* 1986; Atwood, Baldwin, and Carswell 1985, hereafter ABC). To study the internal properties of the intervening clouds and their relation to the surrounding environment (both the radiation field and any possible confining intergalactic medium), it is necessary to use sufficiently high spectral resolution that Voigt profiles may be fitted to the individual absorption lines. The numbers of clouds as a function of H I column density and internal velocity dispersion may then be measured directly. Because the background quasars are faint, large amounts of telescope time are involved, and so this has to date been done in only a few cases (Chaffee *et al.* 1983; Carswell *et al.* 1984; ABC; Chaffee *et al.* 1986).

The results have so far been compatible with models in which the intervening clouds are pressure-confined by a hot intergalactic medium (Sargent *et al.* 1980; Ostriker and Ikeuchi 1983; ABC). Further constraints on this model may be obtained by adding new information on the clouds at the highest observable redshifts. This would allow us to study the evolution of the numbers and column density distribution over a greater range of look-back times, and also probe to the apparent cutoff at redshifts $z \approx 3$–4 in the density of background quasars (Osmer 1982; Green 1986; Koo, Kron, and Cudworth 1987) to see if the intervening clouds become less ionized as a result of the disappearance of the supposed source of the ionizing radiation. In this paper we describe new high-redshift data and investigate the important constraints which they may place on models of the intervening clouds.

II. RESULTS FOR PKS 2000−330

At the time we began this work, the quasar PKS 2000−330 had the highest known redshift ($z = 3.78$; Peterson *et al.* 1982). This quasar is also relatively bright ($m_v \approx 17.3$) and therefore a practical candidate for high-dispersion spectroscopy. Spectra of PKS 2000−330 were obtained using the echelle spectrograph on the CTIO 4 m telescope on the nights of 1984 August 18–22, with a total exposure time of 20.5 hours. A SIT-Vidicon detector was used. The system characteristics have been described by Atwood, Baldwin, and Carswell (1982) and ABC. The resolution over the spectral range 4000–5900 Å is 35 km s^{-1} (FWHM).

[1] Visiting Astronomer, Cerro Tololo Interamerican Observatory.

[2] Cerro Tololo Interamerican Observatory, National Optical Astronomy Observatories, are operated by the Association of Universities for Research in Astronomy, Inc., under contract with the National Science Foundation.

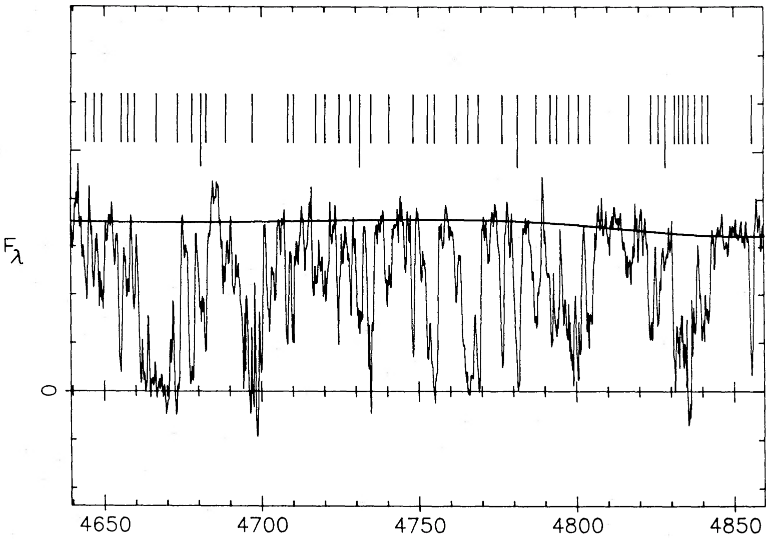

FIG. 1*a*

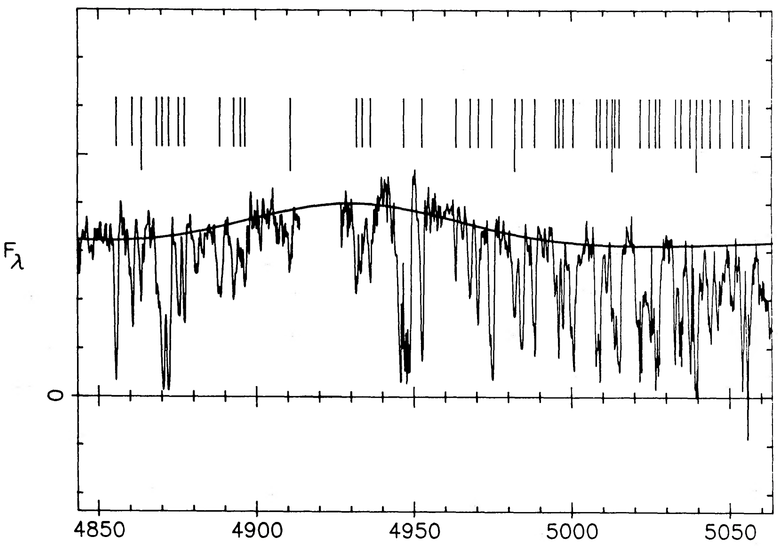

FIG. 1*b*

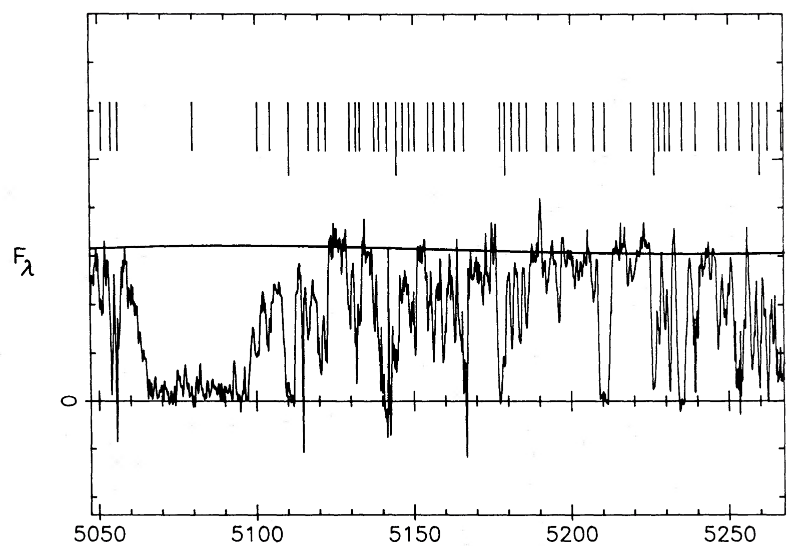

FIG. 1*c*

FIG. 1.—The echelle spectrum of PKS 2000−330, showing the adopted ciontinuum level. Regions of high fixed pattern noise have been masked off. In the region 5380–5420 Å Voigt profiles for Lyα lines with $b = 35$ km s^{-1}, log N(H I) = 13.5, 13.75, 14.0, and 14.5 are shown convolved with the instrument profile for comparison with the data. The tick marks correspond to the wavelengths of the lines given in Table 1.

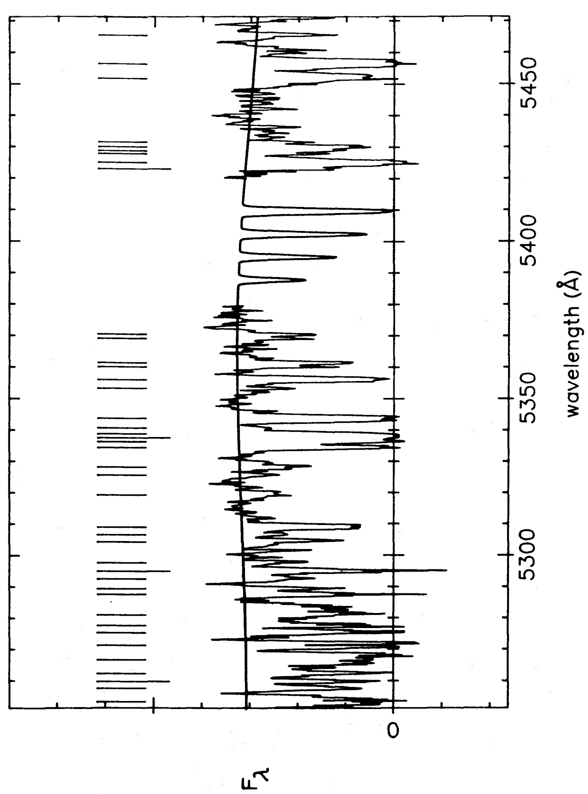

FIG. 1*d*

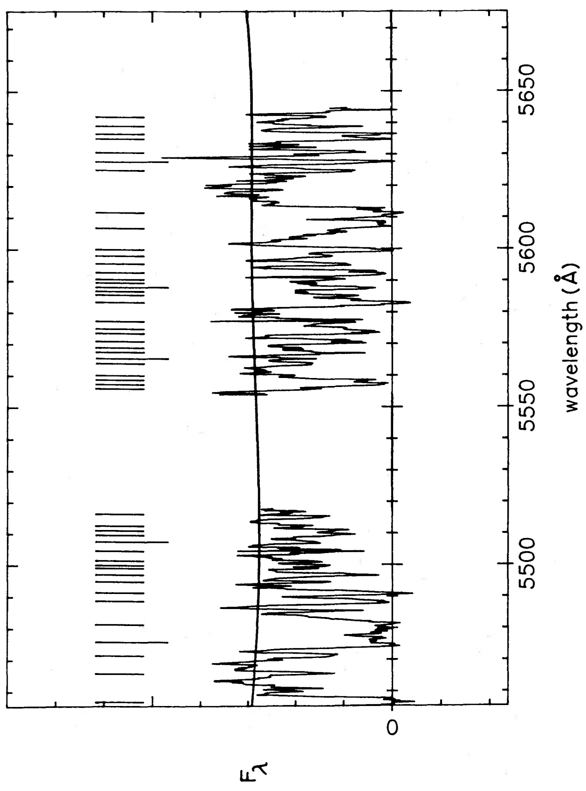

FIG. 1*e*

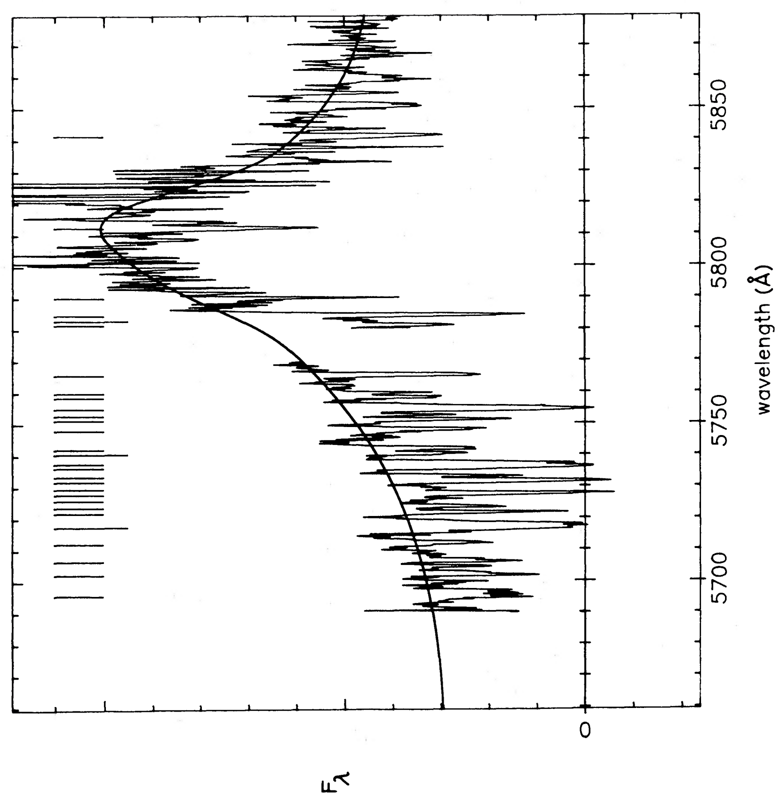

FIG. 1*f*

FIG. 1—*Continued*

At short wavelengths (< 4600 Å) near the center of the detector, there was a high density of discrete background events. Thus in this wavelength region, while there is useful signal over much of the range, our coverage is incomplete. The background events were flagged in the reduction procedure, so the short wavelength region is useful for constraining the profile fits to many of the Lyman series lines but not for generating a line list.

Near the edge of the tube there was a narrow region of bright fixed pattern noise which crossed several echelle orders. This meant that our coverage is also incomplete at long wavelengths near (and shortward of) the Lyα emission line. Figure 1 shows the spectrum of PKS 2000−330 for regions where identification of individual lines was possible, with such noise regions masked off.

With a Lyman line density as high as it is in this object, the continuum level is likely to be very uncertain. We have estimated the continuum using a least-squares spline fit to local continuum levels and have attempted to take into account the presence of weak undetected absorption features. Data points in the spectrum which lie further below a locally determined mean than some chosen threshold are rejected iteratively until the scatter in the remaining normalized residuals does not differ significantly from a normal distribution. The threshold for clipping these data values is chosen so that the number of low values discarded which may be attributed to noise is small, and any removed are likely to be in absorption features. A consistency check is finally made when extracting significant absorption lines by demanding that there are few (spurious) emission features. In general terms the method is similar to that described by Young *et al.* (1979).

The absorption lines were determined against this continuum in the way described by Young *et al.* (1979) and Carswell *et al.* (1982). The (heliocentric) wavelengths, equivalent widths and error estimates are given in Table 1 for wavelengths from 4640 to 5900 Å (Lyγ to just redward of Lyα at the emission redshift). Regions where noise sources in the detector made it impossible to determine the line parameters are indicated in the table.

For Lyman line redshift systems with $z > 3.02$, Voigt profiles convolved with the instrument profile were fitted to obtain the redshift, velocity dispersion, and column density for each ion in each absorbing cloud. Where many lines of an ion are present, all those providing useful constraints have been included in the Voigt profile fit. Table 1 gives the identification, redshift, velocity dispersion ($b = 2^{1/2}\sigma$), and log column density for each component, along with an indication as to which lines were used in the fit, and how badly blending affected these other lines. Thus the content of the table is similar to that for Q0420−388 given by ABC. At redshifts $z < 3.02$ confusion between high-order Lyman lines from higher redshift systems and the candidate Lyα lines makes the parameters for each system less reliable, so they are omitted from this compilation.

There is one significant difference between the way the parameters were determined for PKS 2000−330 here and Q0420−388 by ABC. Instead of a grid search for the minimum χ^2 fit to a feature, we have used a Gauss-Newton type method to search directly for the minimum. For single-component features, this procedure is much quicker and yields results which are in excellent agreement with those obtained using the earlier search technique. It also allows the simultaneous fitting of several components to blends rather than having to extract and fit one component at a time. Error estimates were obtained from the covariance matrix at the best fit values of the parameters. Details of the method are given by Webb (1986).

As in earlier work (Carswell *et al.* 1984; ABC), we have to choose the line sample for determining the distribution functions for the velocity dispersion and column density parameters with some care. We adopt similar criteria to those used by ABC, and for $z > 3.3$ find a H I column density detection limit of log N(H I) = 13.75 for the whole sample if the velocity dispersion $b \geq 5$ km s^{-1}. If there is a significant population of systems with column densities a little above log N(H I) = 13.75, and $b < 5$ km s^{-1}, we would have missed many of them. However, there are no indications from our fits to the data that significant numbers of high column density, low-velocity dispersion systems are present, so there is no reason to suppose that there are many at these lower column densities. So that the errors in the derived quantities are not too large, we choose systems for which the position of at least one Lyman line in addition to Lyα is not badly affected by lines from other (lower redshift) systems, or of too low signal-to-noise ratio (S/N) to provide useful constraints. It is the second requirement which restricts us to considering only those systems with $z > 3.3$ in PKS 2000−330, so that at least Lyβ has adequate S/N. In Table 1 we indicate which lines were used to determine the redshift, N(H I) and b for each system.

For PKS 2000−330, the sample defined as above contains 60 lines, with a mean velocity dispersion $\langle b \rangle = 36.4 \pm 2.5$ km s^{-1}. For comparison, the systems toward Q0420−388 (ABC) yield $\langle b \rangle = 34.4 \pm 1.6$ for the 47 lines selected in the same way. A comparison of the H I column density and velocity dispersion distributions between the two objects was made using the Mann-Whitney U-test. The velocity dispersion distributions were not found to be significantly different, with a 41% probability that they arise from the same parent distribution, while for the column density distributions this probability is 19%. Since for this more reliable subset of the data the distributions for the two objects are not significantly different, we combine the data to yield a sample of 107 systems with a composite column density distribution (Fig. 2) and velocity dispersion distribution (Fig. 3) covering the redshift range $z = 2.72$–3.75.

For the column density distribution a best-fit power law of the form $dp \propto N^{-\beta} dN$ yields $\beta = 1.71$, but a two-sided Kolmogorov-Smirnov test indicates that a power-law fit to these data should be rejected at the 96% level. Evidently there is a flattening of the distribution function towards low column densities. An adequate fit to the data is a continuous function of the form:

$$dp \propto d \log N \quad \text{for} \quad \log N < 14.35 \,,$$
$$dp \propto N^{-1} d \log N \quad \text{for} \quad \log N \geq 14.35 \,.$$

The knee in the N(H I) distribution is potentially a very important tool for following the evolution of these clouds, as will be illustrated in later sections. However, the evidence for it is not overwhelming, and we should consider further whether it is likely to be real or an artifact of our data analysis techniques. There are a number of ways in which a spurious break in the distribution could arise; we consider these in turn.

The first possibility is that the turndown in numbers at low column densities is the result of incompleteness effects setting in at log N(H I) ≈ 14.0. However, as discussed earlier, unless there is a second population of systems with velocity dispersions $b < 5$ km s^{-1}, distinct from those we have detected with a mean velocity dispersion of ~ 35 km s^{-1}, we are likely to have

TABLE 1

ABSORPTION LINES

n	λ_{air}	λ_{vac}	±	EW	±	ID	z	±	b	±	logN	±	Comments
1	4644.06	4645.36	0.12	0.60	0.10								
2	4646.77	4648.07	0.14	0.38	0.09								
3	4649.11	4650.41	0.10	0.93	0.11								
4	4655.36	4656.66	0.06	1.17	0.09								
5	4657.48	4658.79	0.07	0.62	0.08								
6	4659.58	4660.88	0.08	0.51	0.08								
7	4666.50	4667.81	0.07	10.04	0.19								Broad complex
8	4673.23	4674.54	0.04	2.23	0.10								
9	4677.84	4679.15	0.06	1.95	0.11								
10	4680.68	4681.99	0.08	0.84	0.09								
11	4682.34	4683.65	0.08	0.91	0.09								
12	4688.60	4689.91	0.14	0.69	0.10								
13	4697:												
14	4708.30	4709.62	0.06	0.80	0.09								
15	4710.12	4711.44	0.07	0.79	0.09								
16	4717.26	4718.58	0.08	0.77	0.08								
17	4720.16	4721.48	0.09	1.05	0.09								
18	4724.66	4725.98	0.05	0.65	0.06								
19	4728.24	4729.56	0.09	0.61	0.08								
20	4731.23	4732.55	0.07	1.32	0.08								
21	4734.83	4736.15	0.08	1.88	0.12								
22	4740.59	4741.92	0.12	0.99	0.09								
23	4748.28	4749.61	0.07	0.85	0.08								
24	4752.88	4754.21	0.04	1.16	0.07								
25	4755.09	4756.42	0.04	2.29	0.09								
26	4762.03	4763.36	0.10	0.67	0.08								
27	4765.73	4767.06	0.04	3.80	0.10								
28	4769.01	4770.35	0.04	1.64	0.08								
29	4776.58	4777.91	0.06	1.15	0.08								
30	4781.47	4782.80	0.08	2.07	0.11								
31	4787.42	4788.75	0.07	1.48	0.09								
32	4791.88	4793.22	0.06	1.11	0.08								
33	4794.00	4795.34	0.05	1.17	0.08								
34	4797.82	4799.16	0.09	2.65	0.16								Noisy
35	4800.91	4802.25	0.05	1.59	0.09								
36	4804.52	4805.87	0.10	1.51	0.11								
37	4816.85	4818.20	0.15	0.75	0.09								
38	4823.86	4825.21	0.05	1.23	0.08								
39	4826.29	4827.64	0.06	0.81	0.07								
40	4828.44	4829.79	0.12	0.31	0.06								
41	4831.42	4832.77	0.05	1.24	0.08								
42	4832.73	4834.08	0.03	0.82	0.06								
43	4834.07	4835.42	0.03	0.71	0.06								Noisy
44	4835.73	4837.09	0.03	2.22	0.10								"
45	4837.81	4839.16	0.04	0.73	0.06								"
46	4840.14	4841.49	0.06	1.07	0.08								
47	4841.95	4843.31	0.05	0.79	0.06								
48	4855.63	4856.99	0.04	0.96	0.06								
49	4860.64	4861.99	0.07	0.58	0.06								
50	4863.61	4864.97	0.11	0.36	0.06								
51	4868.44	4869.80	0.06	0.20	0.04								
52	4870.22	4871.58	0.03	1.65	0.07								
53	4872.24	4873.60	0.03	1.35	0.06								

TABLE 1—*Continued*

n	λ_{air}	λ_{vac}	±	EW	±	ID	z	±	b	±	logN	±		Comments
54	4875.36	4876.72	0.08	0.69	0.07									
55	4877.23	4878.60	0.05	0.50	0.05									
	Lyβ emission													
56	4888.39	4889.75	0.08	0.84	0.07	Lyα	3.02226	0.00005	63	5	13.68	0.03	α	
57	4892.84	4894.21	0.09	0.73	0.07	Lyα	3.02601	0.00007	55	8	13.60	0.05	α	
58	4895.02	4896.39	0.08	0.31	0.04	Lyα	3.02784	0.00019	44	27	13.29	0.18	α	
59	4896.44	4897.80	0.06	0.41	0.05	Lyα	3.02893	0.00009	25	10	13.34	0.11	α	
60	4910.87	4912.24	0.08	0.42	0.05	Lyα	3.04069	0.00008	45	10	13.38	0.06	α	
	- noise region -	4914 - 4926												
61	4931.85	4933.23	0.08	0.72	0.06	Lyα	3.05790	0.00008	15	17	13.19	0.15	α	
62	4933.75	4935.12	0.07	0.45	0.05	Lyα	3.05888	0.00022	109	17	13.73	0.07	α	
63	4936.36	4937.73	0.09	0.60	0.06	Lyα	3.06166	0.00006	48	7	13.48	0.04	α	
64	4946.91	4948.29	0.07	3.50	0.12	Lyα	3.06830	0.00041	12	73	12.82	0.73	α	Noisy line
						Lyα	3.06942	0.00019	43	28	13.97	0.18	α	
						Lyα	3.07114	0.00031	52	49	14.12	0.25	α	
						Lyα	3.07210	0.00021	9	115	13.79	13.39	α	
65	4952.73	4954.11	0.05	0.89	0.06	Lyα	3.07525	0.00002	23	3	13.93	0.08	α	
66	4963.54	4964.93	0.07	0.21	0.04	Lyα	3.08411	0.00007	5	15	13.24	1.26	α	
67	4968.06	4969.45	0.07	0.50	0.06	Lyα	3.08782	0.00004	31	4	13.47	0.04	α	
68	4970.65	4972.03	0.08	0.57	0.06	Lyα	3.08984	0.00002	16	3	13.59	0.05	α	
69	4974.89	4976.28	0.04	1.38	0.06	Lyα	3.09284	0.00020	7	39	13.54	3.37	α	
						Lyα	3.09357	0.00013	28	10	14.11	0.17	α	
70	4982.16	4983.55	0.06	0.77	0.06	Lyα	3.09942	0.00005	41	5	13.65	0.04	α	
71	4984.41	4985.81	0.04	1.01	0.06	SiII1190	3.18800	0.00004	9	2	13.97	0.33	1190-1304	
72	4988.41	4989.80	0.04	0.81	0.06	SiII1190	3.1914							
73	4995.03	4996.43	0.06	0.28	0.04	Lyα	3.11002	0.00008	14	14	13.21	0.10	α	
74	4996.09	4997.49	0.03	0.51	0.04	SiII1193	3.18800	0.00004	9	2	13.97	0.33	1190-1304	
75	4997.44	4998.84	0.05	0.46	0.05	Lyα	3.11202	0.00004	17	6	13.51	0.08	α	
76	5000.55	5001.95	0.07	1.51	0.08	SiII1193	3.1914							
						Lyα	3.11474	0.00018	14	43	13.65	0.68	αβ	
						Lyα	3.11478	0.00047	58	34	13.78	0.54	α	
77	5008.06	5009.45	0.03	0.66	0.04	Lyα	3.12073	0.00008	11	38	14.17	6.05	α	
78	5009.21	5010.61	0.04	0.86	0.05	Lyα	3.12161	0.00008	23	10	13.90	0.15	α	
79	5011.34	5012.73	0.08	0.28	0.05	Lyα	3.12344	0.00002	18	3	13.20	0.03	α	
80	5013.01	5014.40	0.04	0.29	0.04	Lyα	3.12484	0.00038	7	64	13.39	3.30	α	
81	5013.87	5015.26	0.02	0.57	0.04	Lyα	3.12555	0.00021	26	44	13.72	0.35	α	
82	5015.22	5016.62	0.04	1.17	0.06	Lyα	3.12661	0.00017	32	13	14.00	0.16	α	
83	5021.85	5023.25	0.06	1.67	0.08	Lyα	3.13204	0.00015	64	13	14.03	0.08	α	Noisy
84	5024.69	5026.09	0.05	0.90	0.06	Lyα	3.13474	0.00052	90	67	13.90	0.28	α	"
85	5026.71	5028.11	0.04	1.17	0.07	Lyα	3.13659	0.00019	47	14	14.06	0.19	α	"
86	5028.02	5029.42	0.04	0.61	0.05									
87	5033.02	5034.42	0.04	0.66	0.05	Lyα	3.14122	0.00004	8	11	15.09	5.14	α	
88	5034.79	5036.19	0.06	1.01	0.08	Lyα	3.14268	0.00007	45	7	13.83	0.06	α	
89	5037.61	5039.01	0.08	0.94	0.10	Lyα	3.14505	0.00007	34	6	13.87	0.07	αβ	
90	5039.64	5041.05	0.04	1.50	0.07	Lyα	3.14670	0.00005	29	8	14.31	0.26	αβ	
91	5041.47	5042.88	0.06	0.29	0.04	Lyα	3.14816	0.00010	28	13	13.27	0.10	αβ	
92	5043.98	5045.38	0.05	1.04	0.06	Lyα	3.15033	0.00005	50	6	13.81	0.04	αβ	
93	5047.06	5048.47	0.08	1.12	0.07	Lyα	3.15220	0.00009	15	20	13.28	0.18	α	
						Lyα	3.15294	0.00033	106	25	13.70	0.12	α	
94	5051.04	5052.45	0.08	0.72	0.06	SiIII1206	3.1881							
95	5054.08	5055.49	0.04	1.04	0.06	SiIII1206	3.1914							
96	5056.25	5057.66	0.05	1.57	0.08	Lyα	3.16026	0.00015	58	14	14.00	0.09	α	Noisy

TABLE 1—*Continued*

n	λ_{air}	λ_{vac}	±	EW	±	ID	z	±	b	±	logN	±		Comments
97	5080.	5082.		34.			Not fitted							
98	5100.54	5101.96	0.04	1.97	0.07		″							In wings of
99	5104.56	5105.99	0.06	1.91	0.07		″							5080 feature
100	5110.56	5111.98	0.04	4.24	0.09		″							
101	5116.86	5118.29	0.04	1.02	0.06	Lyα	3.21012	0.00008	65	12	13.85	0.05	$\alpha\beta$	β:1
						Lyα	3.21178	0.00016	25	22	13.16	0.27	$\alpha\beta$	β:1
102	5120.09	5121.51	0.05	1.78	0.09	Lyα	3.21320	0.00008	51	13	14.05	0.06	$\alpha\beta$	β:1
103	5122.27	5123.70	0.03	0.87	0.05	Lyα	3.21473	0.00006	28	6	13.78	0.07	α	
104	5129.76	5131.19	0.05	0.58	0.05	Lyα	3.22089	0.00007	33	8	13.53	0.07	$\alpha\beta$	
105	5131.82	5133.25	0.04	0.82	0.05	Lyα	3.22265	0.00007	26	8	13.82	0.09	$\alpha\beta$	
106	5133.08	5134.51	0.04	0.49	0.04	Lyα	3.22365	0.00009	17	12	13.45	0.11	$\alpha\beta$	
107	5137.58	5139.01	0.05	0.45	0.04	Lyα	3.22732	0.00010	15	17	13.51	0.23	$\alpha\beta$	
108	5139.08	5140.51	0.03	0.92	0.05	Lyα	3.22858	0.00023	30	23	13.81	0.23	$\alpha\beta$	
109	5141.57	5143.00	0.06	3.33	0.09	Lyα	3.23053	0.00016	58	20	14.99	0.42	$\alpha\beta$	
110	5144.58	5146.01	0.03	1.47	0.06	Lyα	3.23299	0.00017	53	21	14.08	0.11	$\alpha\beta$	
111	5146.66	5148.09	0.06	0.42	0.04	Lyα	3.23473	0.00026	33	35	13.26	0.29	$\alpha\beta$	
112	5148.68	5150.12	0.05	0.70	0.05	Lyα	3.23678	0.00022	68	29	13.76	0.12	$\alpha\beta$	
113	5150.39	5151.82	0.04	0.77	0.05	Lyα	3.23804	0.00007	8	15	14.13	3.24	α	
114	5154.75	5156.18	0.05	0.54	0.05	Lyα	3.24144	0.00007	27	8	13.48	0.07	$\alpha\beta$	
115	5156.54	5157.97	0.04	0.86	0.05	Lyα	3.24288	0.00005	31	6	13.77	0.06	$\alpha\beta$	
116	5159.94	5161.38	0.05	1.21	0.07	Lyα	3.24559	0.00007	51	8	13.90	0.05	$\alpha\beta$	
117	5163.12	5164.56	0.04	0.59	0.05	Lyα	3.24835	0.00005	23	7	13.62	0.09	α	
118	5166.13	5167.57	0.07	2.49	0.12	Lyα	3.24976	0.00025	28	21	13.65	0.24	α	Noisy
						Lyα	3.25113	0.00018	42	15	14.23	0.20	α	
119	5177.59	5179.03	0.02	1.64	0.06	Lyα	3.26019	0.00009	31	7	14.31	0.14	$\alpha\beta$	
120	5179.18	5180.62	0.04	0.85	0.05	Lyα	3.26133	0.00016	33	11	13.84	0.14	$\alpha\beta$	
121	5181.38	5182.83	0.06	0.74	0.06	Lyα	3.26335	0.00005	26	6	13.65	0.06	$\alpha\beta$	
122	5183.89	5185.34	0.06	0.83	0.06	Lyα	3.26547	0.00002	28	2	13.70	0.02	α	
123	5186.20	5187.65	0.07	0.65	0.06	Lyα	3.26727	0.00003	34	4	13.57	0.03	α	
124	5192.40	5193.84	0.14	0.38	0.07	Lyα	3.27252	0.00014	48	16	13.23	0.10	α	
125	5196.10	5197.55	0.09	0.54	0.06	Lyα	3.27560	0.00006	34	4	13.57	0.03	α	
126	5201.17	5202.62	0.13	0.21	0.05	Lyα	3.27974	0.00005	16	9	12.98	0.07	α	Marginal
127	5207.30	5208.75	0.12	0.40	0.06	Lyα	3.28473	0.00010	35	12	13.32	0.09	$\alpha\beta$	β:3
128	5210.80	5212.25	0.04	3.63	0.09	Lyα	3.28648	0.00055	26	26	14.04	1.58	$\alpha\beta$	β:3
						Lyα	3.28752	0.00122	50	189	14.36	1.90	$\alpha\beta$	β:3
						Lyα	3.28842	0.00131	33	74	13.90	3.51	$\alpha\beta$	β:3
						Lyα	3.28931	0.00021	10	27	13.15	0.45	$\alpha\beta$	β:3
129	5219.27	5220.72	0.17	0.41	0.07	Lyα	3.29371	0.00005	7	15	12.94	0.29	α	
						Lyα	3.29499	0.00007	39	9	13.07	0.06	α	
130	5226.44	5227.90	0.03	1.50	0.06	Lyα	3.30040	0.00006	36	7	14.15	0.11	$\alpha\beta$	Noisy
131	5228.03	5229.49	0.04	0.51	0.05	Lyα	3.30174	0.00009	17	12	13.54	0.14	$\alpha\beta$	
132	5229.89	5231.34	0.05	0.50	0.05	Lyα	3.30330	0.00004	23	6	13.52	0.06	$\alpha\beta$	
133	5231.40	5232.86	0.04	0.95	0.06	Lyα	3.30454	0.00003	17	3	14.20	0.17	$\alpha\beta$	
134	5235.25	5236.70	0.04	3.03	0.09	Lyα	3.30723	0.00040	37	21	14.45	0.91	$\alpha\beta$	β:1
						Lyα	3.30791	0.00135	58	28	14.33	1.14	$\alpha\beta$	β:1
135	5239.59	5241.05	0.08	1.31	0.09	Lyα	3.31120	0.00012	48	12	13.91	0.10	α	Noisy
136	5246.96	5248.42	0.06	0.74	0.06	Lyα	3.31726	0.00004	26	5	13.65	0.05	α	
137	5249.27	5250.73	0.08	0.83	0.07	Lyα	3.31915	0.00008	60	8	13.67	0.04	α	
138	5253.42	5254.88	0.06	2.90	0.10	Lyα	3.32260	0.00008	77	8	14.42	0.08	α	Noisy
139	5257.64	5259.10	0.05	1.18	0.07	Lyα	3.32610	0.00005	38	5	14.01	0.05	$\alpha\beta$	β:1
140	5259.80	5261.26	0.04	1.16	0.07	Lyα	3.32787	0.00004	30	4	14.27	0.08	$\alpha\beta$	
141	5262.35	5263.81	0.04	1.48	0.07	Lyα	3.32996	0.00008	41	8	14.02	0.08	α	
142	5266.69	5268.15	0.07	4.15	0.15	Lyα	3.33314	0.00028	117	20	14.41	0.09	α	
						Lyα	3.33479	0.00016	20	45	14.98	6.38	α	
143	5271.33	5272.79	0.04	2.50	0.10	Lyα	3.33735	0.00008	27	35	16.04	6.29	α	Double?

TABLE 1—*Continued*

n	λ_{air}	λ_{vac}	±	EW	±	ID	z	±	b	±	logN	±		Comments
144	5275.39	5276.86	0.04	1.59	0.08	Lyα	3.34077	0.00006	32	8	14.24	0.21	$\alpha\beta$	β:2
145	5277.73	5279.20	0.04	1.42	0.07	Lyα	3.34254	0.00007	39	8	14.01	0.08	$\alpha\beta$	β:2 Noisy
146	5281.06	5283.53	0.07	3.00	0.11	Lyα	3.34602	0.00021	115	19	14.27	0.07	$\alpha\beta$	β:2
147	5287.65	5289.12	0.05	1.33	0.08	Lyα	3.35075	0.00007	33	8	14.06	0.14	α	
148	5289.46	5290.93	0.05	0.61	0.05	Lyα	3.35229	0.00005	21	7	13.59	0.09	$\alpha\beta$	β:1
149	5292.58	5294.05	0.06	0.63	0.06	Lyα	3.35497	0.00013	50	14	13.56	0.09	$\alpha\beta$	β:1
150	5295.05	5296.52	0.05	1.79	0.09	Lyα	3.35691	0.00006	38	7	14.18	0.12	$\alpha\beta$	β:1 Noisy
151	5297.73	5299.20	0.06	0.46	0.06	Lyα	3.35917	0.00007	26	9	13.39	0.08	α	
152	5304.36	5305.84	0.06	0.98	0.08	Lyα	3.36487	0.00006	30	7	13.69	0.07	$\alpha\beta$	
153	5306.69	5308.16	0.08	0.40	0.06	Lyα	3.36646	0.00004	37	5	13.33	0.03	α	
154	5309.09	5310.56	0.05	1.68	0.08	Lyα	3.36842	0.00005	50	5	14.11	0.05	$\alpha\gamma$	
155	5319.33	5320.81	0.14	0.60	0.08	Lyα	3.37698	0.00013	73	13	13.47	0.06	$\alpha\beta$	
156	5325.71	5327.19	0.13	0.26	0.06	Lyα	3.38213	0.00006	22	7	13.08	0.06	α	
157	5328.27	5329.75	0.10	0.71	0.07	Lyα	3.38428	0.00012	61	14	13.62	0.07	α	
158	5334.50	5335.98	0.03	1.65	0.07	Lyα	3.38938	0.00004	29	3	14.48	0.12	$\alpha\beta$	β:4
159	5336.38	5337.87	0.02	1.45	0.05	Lyα	3.39081	0.00035	21	25	14.33	0.65	$\alpha\beta$	β:4
160	5337.63	5339.12	0.01	1.00	0.04	Lyα	3.39175	0.00069	45	130	14.35	1.15	$\alpha\beta$	β:4
161	5338.91	5340.39	0.03	1.49	0.06	Lyα	3.39280	0.00026	27	12	14.75	0.39	$\alpha\beta$	β:4
162	5340.77	5342.25	0.12	0.24	0.05	Lyα	3.39436	0.00019	42	22	13.16	0.15	$\alpha\beta$	β:4
163	5343.85	5345.33	0.06	2.74	0.10	Lyα	3.39693	0.00002	47	2	14.66	0.06	$\alpha\beta$	β:1
164	5353.37	5354.86	0.08	0.31	0.05	Lyα	3.40484	0.00003	12	5	13.28	0.07	α	
165	5356.12	5357.61	0.04	1.96	0.08	Lyα	3.40718	0.00003	33	2	14.60	0.09	$\alpha\beta$	β:1
166	5360.17	5361.66	0.05	0.52	0.05	Lyα	3.41406	0.00011	15	15	13.51	0.20	$\alpha\beta$	
167	5361.51	5363.00	0.04	0.93	0.06	Lyα	3.41157	0.00008	28	10	13.82	0.10	$\alpha\beta$	
168	5369.20	5370.69	0.05	0.37	0.05	Lyα	3.41788	0.00004	13	7	13.40	0.09	α	
169	5370.59	5372.09	0.09	0.60	0.07	Lyα	3.41894	0.00004	22	5	13.51	0.04	α	
	- noise region -		5380 - 5420											
170	5423.09	5424.60	0.05	0.47	0.05	Lyα	3.46219	0.00016	14	23	13.26	0.24	$\alpha\beta$	
171	5425.20	5426.71	0.04	2.91	0.10	Lyα	3.46387	0.00008	60	7	14.54	0.06	$\alpha\beta$	
172	5427.99	5429.50	0.05	0.46	0.05	SiII1193	3.55003	0.00005	15	6	13.13	0.09	1020-1304	1020:1
173	5428.96	5430.47	0.03	0.46	0.05	Lyα	3.46714	0.00021	21	16	13.53	0.27	$\alpha\beta\delta$	β:1
174	5430.22	5431.73	0.04	1.26	0.07	Lyα	3.46811	0.00014	34	13	13.97	0.12	$\alpha\beta\gamma\delta$	β:1
175	5431.74	5433.25	0.07	0.32	0.06	Lyα	3.46933	0.00009	12	14	13.23	0.15	$\alpha\beta\gamma\delta$	β:1
176	5451.92	5453.43	0.08	2.95	0.13	Lyα	3.48421	0.00028	41	24	13.26	0.24	$\alpha\beta\gamma$	β:3
						Lyα	3.48627	0.00009	71	8	14.31	0.05	$\alpha\beta\gamma$	β:3 OI 3.1881
177	5456.62	5458.13	0.05	3.46	0.12	Lyα	3.48987	0.00004	58	4	14.77	0.08	$\alpha\beta\gamma$	β:3 OI 3.1914
178	5465.58	5467.09	0.11	0.59	0.09	SiII1304	3.1914							
179	5471.27	5472.79	0.09	0.94	0.10	Lyα	3.50197	0.00006	31	7	13.74	0.07	α	
180	5475.56	5477.08	0.05	3.70	0.12	Lyα	3.50460	0.00016	36	9	14.39	0.27	$\alpha\gamma\delta$	γ:2
						Lyα	3.50611	0.00021	48	29	14.22	0.26	$\alpha\gamma\delta$	γ:2
181	5481.09	5482.61	0.08	5.69	0.16	Lyα	3.50856	0.00060	85	63	14.53	0.32	$\alpha\gamma\delta$	γ:2
						Lyα	3.51020	0.00033	37	32	14.24	0.57	$\alpha\gamma\delta$	γ:2
						Lyα	3.51146	0.00076	61	41	13.81	0.42	$\alpha\gamma\delta$	γ:2
182	5488.51	5490.04	0.05	1.82	0.10	Lyα	3.51603	0.00006	43	7	14.17	0.08	$\alpha\beta$	
183	5491.17	5492.69	0.05	1.83	0.10	Lyα	3.51822	0.00006	37	5	14.24	0.09	$\alpha\beta$	
184	5494.64	5496.17	0.06	0.32	0.06	Lyα	3.52110	0.00006	7	3	13.64	0.31	$\alpha\beta$	
185	5496.84	5498.36	0.08	1.12	0.10	Lyα	3.52292	0.00004	28	4	13.88	0.06	$\alpha\beta$	
186	5498.91	5500.44	0.07	0.28	0.06	Lyα	3.52460	0.00006	7	3	13.64	0.31	$\alpha\beta$	
187	5499.84	5501.37	0.05	0.47	0.06	Lyα	3.52535	0.00009	15	14	13.49	0.13	$\alpha\beta$	
188	5501.30	5502.83	0.11	0.47	0.08	Lyα	3.52639	0.00007	7	22	13.63	2.81	α	
189	5504.40	5505.93	0.11	0.86	0.12	Lyα	3.52909	0.00015	41	15	13.78	0.14	$\alpha\beta$	Noisy
190	5507.32	5508.85	0.08	0.51	0.08	Lyα	3.53151	0.00006	25	7	13.45	0.07	$\alpha\beta$	β:2
191	5509.46	5510.99	0.07	0.94	0.10	Lyα	3.53350	0.00009	46	9	13.83	0.06	$\alpha\beta$	β:2
192	5510.93	5512.46	0.05	0.67	0.08	Lyα	3.53459	0.00005	7	3	14.10	0.47	$\alpha\beta$	β:2
193	5512.41	5513.94	0.13	0.37	0.08	Lyα	3.53566	0.00008	27	9	13.27	0.08	$\alpha\beta$	β:2

TABLE 1—*Continued*

n	λ_{air}	λ_{vac}	±	EW	±	ID	z	±	b	±	logN	±		Comments
194	5516.15	5517.68	0.19	0.95	0.14	Lyα	3.53801	0.00005	22	6	13.48	0.07	$\alpha\gamma$	γ:1
						Lyα	3.53931	0.00010	22	14	13.13	0.12	$\alpha\gamma$	γ:1
	- noise region -	5518 - 5554												
195	5555.74	5557.28	0.05	0.32	0.05	Lyα	3.57137	0.00011	5	11	13.40	1.51	$\alpha\beta$	β:2
196	5557.12	5558.66	0.03	1.35	0.08	Lyα	3.57251	0.00023	31	17	14.04	0.21	$\alpha\beta$	β:2
197	5558.56	5560.10	0.04	0.96	0.08	Lyα	3.57357	0.00031	35	19	13.90	0.26	$\alpha\beta$	β:2
198	5559.97	5561.51	0.07	0.22	0.05	Lyα	3.57485	0.00012	4	11	13.19	1.60	$\alpha\beta$	β:2
199	5563.73	5565.27	0.10	0.55	0.08	Lyα	3.57795	0.00006	31	6	13.30	0.06	$\alpha\gamma$	γ:1
200	5565.30	5566.85	0.08	0.26	0.06	Lyα	3.57925	0.00005	6	9	13.30	0.82	$\alpha\gamma$	γ:1
201	5567.31	5568.86	0.06	0.79	0.08	Lyα	3.58074	0.00011	21	15	13.66	0.14	α	
202	5568.73	5570.28	0.08	0.24	0.06	Lyα	3.58187	0.00023	26	30	13.25	0.23	α	
203	5570.71	5572.26	0.05	1.24	0.09	Lyα	3.58372	0.00008	38	8	13.94	0.08	α	
204	5573.26	5574.81	0.06	0.63	0.08	Lyα	3.58605	0.00018	21	22	13.76	0.39	$\alpha\beta$	β:2
205	5574.68	5576.23	0.04	1.47	0.09	Lyα	3.58683	0.00043	60	21	14.02	0.22	$\alpha\beta$	β:2
206	5577.07	5578.62	0.10	1.13	0.12	Lyα	3.58890	0.00032	56	24	13.74	0.16	$\alpha\beta$	β:2
207	5583.09	5584.64	0.04	2.55	0.11	Lyα	3.59366	0.00010	40	9	14.31	0.11	$\alpha\beta\delta$	β:2,δ:1
						Lyα	3.59480	0.00014	9	7	13.72	0.30	$\alpha\beta\delta$	β:2,δ:1
208	5585.43	5586.98	0.05	0.86	0.07	Lyα	3.59568	0.00010	26	14	13.70	0.10	$\alpha\beta\delta$	β:2,δ:1
209	5586.59	5588.15	0.05	0.21	0.05	Lyα	3.59662	0.00015	5	8	13.28	0.59	$\alpha\beta\delta$	β:2,δ:1
210	5587.87	5589.42	0.04	1.25	0.08	Lyα	3.59762	0.00011	27	13	13.87	0.24	$\alpha\beta\delta$	β:2,δ:1
211	5589.29	5590.84	0.05	0.29	0.05	Lyα	3.59891	0.00059	65	108	13.66	0.59	$\alpha\beta\delta$	β:2,δ:1
212	5590.40	5591.95	0.05	0.66	0.07	Lyα	3.60003	0.00007	10	14	13.65	0.44	$\alpha\beta\delta$	β:2,δ:1
213	5592.51	5594.06	0.05	1.87	0.11	CII1334	3.19146	0.00017	19	14	14.57	0.63	1036,1334	1036:1
214	5595.32	5596.87	0.06	0.86	0.09	Lyα	3.60198	0.00017	28	12	13.90	0.18	$\alpha\beta$	
215	5597.79	5599.35	0.06	0.89	0.09	Lyα	3.60596	0.00016	39	14	13.63	0.11	$\alpha\beta$	β:1
216	5599.80	5601.36	0.05	1.69	0.11	Lyα	3.60757	0.00008	38	7	14.23	0.12	$\alpha\beta$	β:1
217	5606.53	5608.09	0.09	4.29	0.17	Lyα	3.61043	0.00036	37	29	13.33	0.31	$\alpha\beta\gamma\delta$	β:2,γ:1
						Lyα	3.61208	0.00024	53	36	13.83	0.22	$\alpha\beta\gamma\delta$	β:2,γ:1
						Lyα	3.61410	0.00007	49	5	14.80	0.05	$\alpha\beta\gamma\delta$	β:2,γ:1
218	5611.43	5612.98	0.06	3.65	0.14	Lyα	3.61686	0.00017	46	9	14.64	0.15	$\alpha\beta\gamma\delta$	β:2,γ:1
						Lyα	3.61833	0.00014	19	8	14.15	0.22	$\alpha\beta\gamma\delta$	β:2,γ:1
219	5624.89	5626.45	0.08	0.93	0.10	Lyα	3.62821	0.00004	20	4	13.92	0.08	$\alpha\beta\gamma$	
220	5627.62	5629.18	0.05	1.25	0.11	Lyα	3.63051	0.00004	22	6	14.21	0.36	$\alpha\beta\epsilon$7	β:1,7:2
221	5630.57	5632.13	0.06	1.10	0.11	Lyα	3.63313	0.00005	18	4	14.04	0.11	$\alpha\beta\epsilon$	
222	5634.88	5636.45	0.05	1.28	0.10	Lyα	3.63652	0.00006	20	12	14.38	0.94	$\alpha\beta$7	
223	5636.44	5638.00	0.06	1.14	0.10	Lyα	3.63773	0.00006	16	4	14.76	0.57	$\alpha\beta$7	
224	5638.93	5640.50	0.11	0.84	0.12	Lyα	3.63977	0.00005	25	5	13.70	0.07	$\alpha\beta$7	
225	5641.85	5643.42	0.08	0.56	0.09	Lyα	3.64218	0.00008	34	9	13.55	0.07	$\alpha\beta$7	
	- noise region -	5645 - 5690												
226	5695.65	5697.23	0.14	1.61	0.17	Lyα	3.68659	0.00012	74	10	13.94	0.05	$\alpha\gamma$	γ:3
227	5702.20	5703.78	0.10	0.83	0.12	Lyα	3.69159	0.00054	13	37	13.50	0.79	$\alpha\beta$	
						Lyα	3.69224	0.00143	23	94	13.21	1.53	$\alpha\beta$	
228	5706.50	5708.09	0.08	0.64	0.10	Lyα	3.69542	0.00012	28	13	13.50	0.12	$\alpha\beta$	β:1
229	5712.11	5713.69	0.12	0.47	0.10	Lyα	3.70014	0.00011	17	14	13.36	0.15	$\alpha\beta$	
230	5717.41	5719.00	0.08	2.79	0.16	Lyα	3.70362	0.00013	11	9	14.01	0.40	$\alpha\beta\epsilon$	β:1
						Lyα	3.70466	0.00020	45	12	14.32	0.16	$\alpha\beta\epsilon$	β:1
231	5721.85	5723.43	0.09	0.77	0.11	Lyα	3.70810	0.00003	8	2	15.29	0.37	$\alpha\gamma\epsilon$	γ:1
232	5723.67	5725.26	0.12	0.56	0.11	Lyα	3.70958	0.00007	20	8	13.49	0.09	$\alpha\beta$	
233	5725.85	5727.43	0.22	0.26	0.10	Lyα	3.71151	0.00016	29	18	13.13	0.15	$\alpha\gamma$	γ:1
234	5727.77	5729.36	0.06	1.40	0.12	Lyα	3.71291	0.00005	19	5	14.50	0.51	$\alpha\gamma$	γ:1
235	5729.50	5731.09	0.13	0.27	0.09	Lyα	3.71428	0.00018	30	20	13.16	0.16	$\alpha\gamma$	γ:1
236	5731.78	5733.37	0.06	1.62	0.12	Lyα	3.71623	0.00006	27	5	14.29	0.15	$\alpha\gamma$	
237	5733.39	5734.98	0.06	0.49	0.08	SiII1260	3.55003	0.00005	15	6	13.13	0.09	1020-1304	1020:1

TABLE 1—*Continued*

n	λ_{air}	λ_{vac}	±	EW	±	ID	z	±	b	±	logN	±		Comments
238	5736.16	5737.75	0.04	1.42	0.10	Lyα	3.71961	0.00022	16	12	14.14	0.42	αβ8	β:1
239	5737.50	5739.09	0.04	1.03	0.09	Lyα	3.72044	0.00027	37	11	14.52	0.18	αβ8	β:1
240	5740.49	5742.09	0.09	0.47	0.09	Lyα	3.72342	0.00018	27	21	13.37	0.16	αβγ	
241	5742.06	5743.66	0.08	0.57	0.09	Lyα	3.72469	0.00016	23	19	13.39	0.15	αβγ	
242	5748.04	5749.64	0.14	0.76	0.13	Lyα	3.72967	0.00012	31	12	13.48	0.11	αβ	
243	5751.28	5752.88	0.09	0.68	0.10	Lyα	3.73232	0.00010	23	11	13.50	0.11	αβγδ	β:4,γ:1
244	5752.74	5754.34	0.10	0.34	0.08	Lyα	3.73348	0.00014	16	18	13.14	0.18	αβγδ	β:4,γ:1
245	5754.91	5756.51	0.07	2.11	0.14	Lyα	3.73521	0.00003	29	2	14.73	0.07	αβγδ	β:4,γ:1
246	5758.47	5760.07	0.10	0.48	0.09	Lyα	3.73821	0.00010	23	11	13.33	0.11	αβ	
247	5759.91	5761.51	0.16	0.30	0.09	Lyα	3.73936	0.00005	4	2	13.96	0.60	αβ	
248	5765.54	5767.14	0.08	0.81	0.10	Lyα	3.74395	0.00008	27	8	13.64	0.09	αβ	
	- noise	region -	5770 -	5780										
249	5781.46	5783.07	0.05	0.80	0.08	Lyα	3.75672	0.00020	38	21	13.65	0.17	αβ	β:1
250	5782.88	5784.48	0.06	0.41	0.07	Lyα	3.75828	0.00034	38	47	13.32	0.40	αβ	β:1
251	5784.58	5786.18	0.06	1.18	0.09	Lyα	3.75971	0.00007	28	6	13.94	0.07	αβ	β:1
252	5790.10	5791.70	0.07	0.42	0.06	Lyα	3.76424	0.00007	20	8	13.33	0.08	αβ	
253	5812.36	5813.97	0.06	0.66	0.06	Lyα	3.78252	0.00008	38	8	13.50	0.06	αβ	
						Lyα	3.78406	0.00010	18	13	13.09	0.11	αβ	
254	5841.32	5842.94	0.07	0.71	0.08	SiIV1393	3.19226	0.00007	34	7	13.36	0.06	1393-1402	

NOTES.—Heliocentric observed wavelengths and equivalent widths are given in Å. The errors quoted after each measured quantity are 1 σ estimates. Vertical bars indicate blended features. If more than one Lyman line in any redshift system falls in the observed wavelength range, the positions of all the Lyman lines, except those badly affected by blends from lines at other redshifts, are used to determine z, b, and N. The Greek letters in the comments column indicate which Lyman lines were used in each case, and the numbers after the colons give the number of Lyα lines blended with the indicated higher order line.

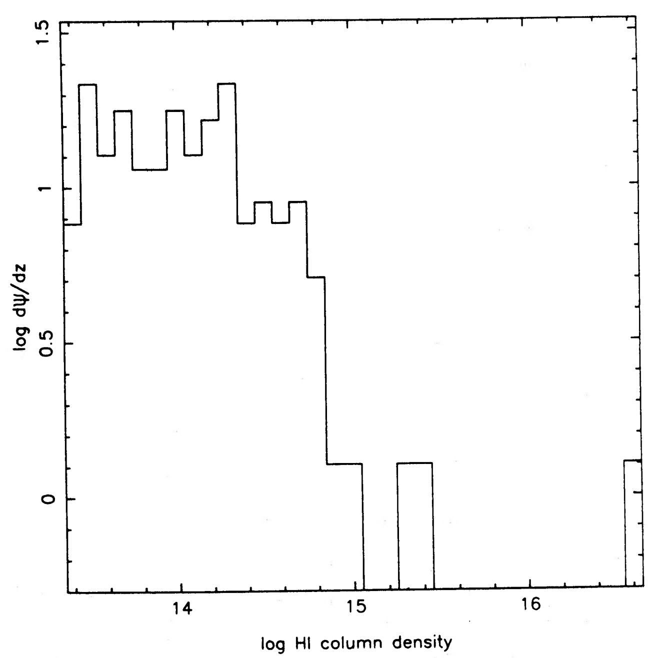

FIG. 2

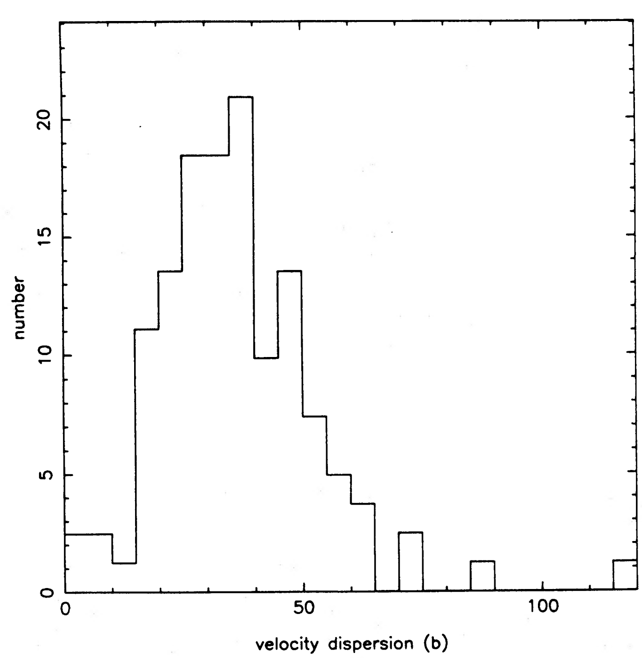

FIG. 3

FIG. 2.—The H I column density distribution for the redshift range $2.72 < z < 3.73$. The vertical scale is arbitrary, since only systems for which at least two Lyman lines were available for profile fitting were included in the compilation. The lowest values correspond to a single point in that log N bin. If no value is shown, the bin is empty.

FIG. 3.—The velocity dispersion distribution for $2.72 < z < 3.75$. The vertical scale gives the number of systems per velocity bin in Q0420−388 and PKS 2000−330, subject to the constraints given in the test.

missed very few systems in the range $13.75 < \log N < 14.0$ unless they are themselves covered by higher column density systems. Correcting properly for this effect requires analysis of simulated data, but we can make an approximate correction by determining the fraction of the spectrum over which high column density systems may mask weaker components. We estimate that at the most 10% of systems with $\log N < 14.0$ could have been masked in this way. If we suppose that 10% of the low column density systems are missed, then, correcting approximately for this, we find that a best-fit power law with $\beta \sim 1.76$ has 9% chance of being applicable.

A second point is that we could be biassing against low column density systems by setting the continuum level too low. If, for example, Lyα is the dominant line in determining all the system parameters, then for lines with high optical depths the inferred H I column densities would be little changed if we were to set the continuum level higher or lower, but the low optical depth systems could suffer significant changes. To test this possibility we set the continuum level everywhere to be 15% higher than the adopted value shown in Figure 1 and redetermined system parameters for the redshift range $3.68 < z < 3.74$. We found that on average $\log N$ increased by 0.2, with little dependence on the Lyα line depth. This insensitivity to line depth is probably because N(H I) for most systems is best constrained by the optically thin lines of the Lyman series, and so the continuum change in the region of these dominates the results. Thus an error in the continuum level should not significantly affect the detectability of a knee in the N(H I) distribution, though it may strongly affect our measurement of its position.

A third point is that we may have underfitted our data by choosing as few components as an acceptable χ^2 allows. For high column density systems where several Lyman lines are measured, this is unlikely to be a problem, but at low column densities the inferred number of components in a blend depends almost solely on the Lyα line profile. Thus if we have underfitted the data we could have underestimated the number of weak systems. It is difficult to rule out this possibility completely, since the data variances used to determine the χ^2 values were obtained by examining the noise characteristics in the difference between two exposures and then correcting this to the sum of all the data, so are themselves approximate. However, the distribution of χ^2 values suggests that there is no significant under- or overfitting of the spectral lines.

A final possibility is that we might be missing a few high H I column density systems because the S/N in the region covering most of the high-order Lyman lines is poorer than for Lyα, and we may have allowed more lower redshift Lyα components blended with these than are required. The number of systems involved is small, so such a bias might not affect our tests for under- or overfitting significantly. Under these circumstances the N(H I) distribution would be flatter than our data have indicated, and so the deviation from a power law at low column densities less significant. Any high column density systems must have Lyα lines with central intensities close to zero, so only those systems for which our estimate $\log N > 14.3$ or so could be affected. To test such a bias we have taken all our lines for which $\log N > 14.4$ and for half of them added up to 0.4 to $\log N$, and then redetermined the distribution function. This is somewhat rough, but will give a guide as to the possible behavior. The best-fit power law tends to be somewhat flatter, with trials giving $\beta \approx 1.65$ and a chance probability of such a power law describing the data ~ 3 times higher than before at $\sim 11\%$. On the other hand errors in the N(H I) determinations due to finite S/N in the data would be likely to give more spurious high column density systems from Malmquist bias. Under these circumstances the true high column density distribution index may have an even larger negative value.

Any or all of these considerations, with some statistical fluctuation in the measured N(H I) distribution, may reduce, to some extent, the significance of our suggested knee in the distribution. However, none has a very large effect, so the tentative evidence for a break in the power law remains. Confirmation, or denial, of its reality can come only with further data and simulations to allow for systematic biasses.

The velocity dispersion distribution function for the combined data for Q0420−388 and PKS 2000−330, covering a redshift range $2.72 < z < 3.745$, with the sample subject to the same restrictions as above, has a mean value $\langle b \rangle = 35.8 \pm 1.3$ km s^{-1} and $\sigma = 16.5$ km s^{-1}. This measure of the width of the b distribution is close to the mean value of the error estimate from the Voigt profile fitting procedure, which yields $\langle \sigma_b \rangle = 13.3$ km s^{-1}. Possibly, then, the apparent dispersion in the values for b is largely due to measurement errors, and so a single velocity dispersion may apply to most of the clouds in the redshift range. If this result is correct, it could be an important constraint for the cloud models (see below). Confirmation would require higher resolution data with good S/N and coverage of as many lines of the Lyman series as possible.

III. LYMAN-ALPHA CLOUD SAMPLE

We now combine the high-dispersion spectroscopic results for PKS 2000−330 with those already published for Q0420−388 (ABC) and Q1101−264 ($z_{em} = 2.14$; Carswell *et al.* 1984) to investigate the cloud properties over the widest available range of redshift. Within the spectrum of each quasar, the redshift range is limited at the upper end by the requirement that we do not take redshifts so high that the background quasar would itself be the primary source of ionization. Thus the redshift ranges used were $z = 1.88$–1.98 and $z = 2.04$–2.09 in Q1101−264; $z = 2.72$–3.08 in Q0420−388; and the sections of PKS 2000−330 given in Table 1 in the range $3.30 < z < 3.745$. Although the intervening clouds toward these quasars are along radically different lines of sight, it is reasonable to combine the individual samples since the available evidence indicates that most of the clouds are extrinsic to the quasars and that there are no gross inhomogeneities in the universe.

For each of these quasars we include systems down to a uniform column density limit $\log N(\text{H I}) > 13.75$. In examining the redshift evolution of the *numbers* of clouds we must include all systems above the threshold, so cannot exclude those for which blending of the high-order Lyman lines prevents us from determining b and N(H I) reliably, as was done to determine the shapes of the distribution functions in § II. If the number of systems per unit redshift $d\Psi/dz \propto (1+z)^\gamma$, then for this sample we find the maximum likelihood $\gamma = 1.03 \pm 0.59$ for 152 Lyman line systems. This result is critically dependent on the small number of systems (17, in two wavelength regions) satisfying the criteria in the $z = 2.14$ QSO Q1101−264, and for this reason the formal error quoted is probably an underestimate. If we include the additional high-resolution material from Webb (1986) to improve the sample size at low redshifts, then we find $\gamma = 1.76 \pm 0.46$.

Our estimates for γ are lower than $\gamma = 2.36 \pm 0.36$ obtained by Chen *et al.* (1984), or $\gamma = 2.31 \pm 0.40$ by Hunstead *et al.* (1986), both using larger numbers of spectra, but at significantly lower resolution, and adopting an equivalent width limited line sample. It is not obvious that these estimates for γ should necessarily agree with ours. Many of the lines detected at intermediate dispersion with rest equivalent widths greater than 0.32 Å turn out to be blends of weaker lines, as is seen by comparing published data at 1.5 Å and <0.5 Å resolution on two objects (Q1101−264: Carswell *et al.* 1982 and Carswell *et al.* 1984; PKS 2000−330: Hunstead *et al.* 1986, and the data given here). This blending problem should be more severe at high redshifts than low, even in a nonevolving cloud model, but it is not clear if this increases or decreases the apparent redshift evolution of their numbers. It is also quite likely that the form of the evolution for the total number of lines above some detection threshold is a function of the chosen threshold value, since, as discussed below, the redshift evolution of the N(H I) distribution function need not be a simple scaling.

Consideration of the total number of lines cannot provide us with as much information as we would obtain by examining the N(H I) distribution function as a function of redshift. Only if the distribution is a power law will we learn nothing new from examining the distribution in detail, but for more complex forms we can obtain some indications of how clouds of a particular N(H I) evolve. With the N(H I) distribution determined in § II, we may now illustrate this. Using data from PKS 2000−330 and Q0420−388, we find that the column density at which the possible knee in this distribution occurs may shift slightly between $z = 3.5$ and $z = 2.9$. We find that the

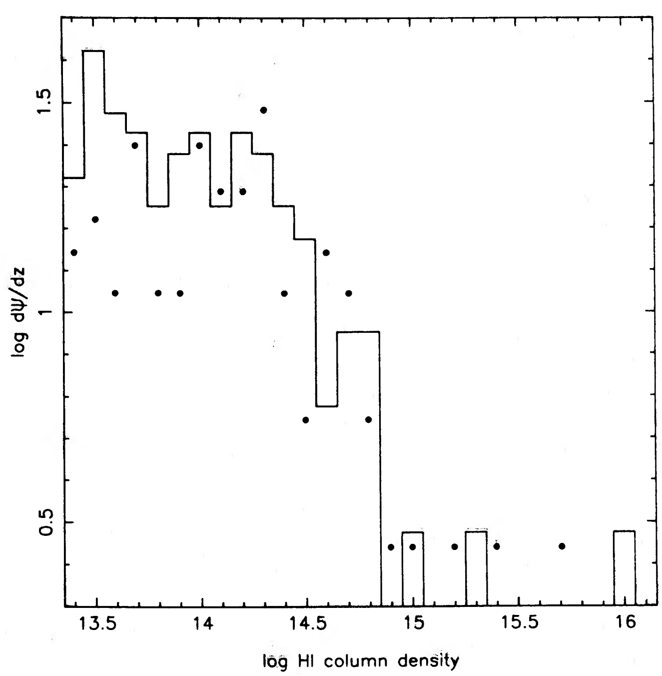

FIG. 4.—The observed H I column density distribution at $\langle z \rangle = 3.5$ from PKS 2000−330 (*histogram*) and $\langle z \rangle = 2.9$ from Q0420−388. The vertical scale gives the numbers of systems per unit redshift per $\Delta \log N = 0.1$. The lowest values in each case correspond to a single point in that log N bin. If no value is shown, then the bin is empty. The adopted completeness limit is log $N = 13.75$.

probability that the two distributions are the same (using a Mann-Whitney U-test) is at a maximum when the shift is $\Delta \log N \approx 0.15$ so that a value $\log N$ at $z = 3.5$ becomes $\log N + 0.15$ at $z = 2.9$. However, the errors in this quantity are large, with a 95% confidence interval $-0.1 < \Delta \log N < 0.4$, so the data are consistent with zero shift. Possible systematic errors in the H I column densities arising from uncertainties in the continuum level, as discussed in § II, make the uncertainties even larger, so the range in $\Delta \log N$ may be from -0.3 to $+0.6$. To obtain the normalization for the distribution function at the two mean redshifts we count systems with N(H I) above the threshold so that the minimum $\log N > 13.75$ is satisfied for both objects. We then find that the normalization changes to 0.8 of its value at $z = 3.5$ by the time $z = 2.9$, but at the ends of the allowed range in $\Delta \log N$ this factor is 0.3 and 1.4. In instead we compare relative heights of the flat portions of both distributions over the range $13.75 < \log N < 14.25$, we find that the normalization at $z = 2.9$ is 0.8 ± 0.2 times its value at $z = 3.5$. Figure 4 shows the N(H I) distributions for the two redshift ranges. The data at lower redshifts, from Q1101−264, is too sparse to allow even tentative comparisons.

ABC have described simple models in which a comoving population of uniform clouds is responsible for the Lyman line absorption. They assumed that the masses of individual clouds do not change with redshift and showed that, if all clouds behave similarly, knowledge of the shape of the N(H I) distribution function and redshift dependence of the cloud numbers can constrain models of the cloud evolution. If a knee is present in the N(H I) distribution we may infer the redshift dependence of the H I column density for particular clouds, and so infer the behavior of the density and neutral hydrogen fraction. To do this we follow ABC's formalism with certain corrections.[3]

The important difference from the ABC treatment is that the H I column density distribution is now found not to be adequately fitted by a power law, so it is necessary to allow for a more general distribution. For a comoving population of clouds, the number of mass m and redshift z along a sight line is

$$d\Psi(m, z) = \frac{\Gamma c}{H_0} \frac{y^2(1+z)}{(1+2q_0 z)^{1/2}} f(m) dm dz , \tag{1}$$

where y is the characteristic length scale for a cloud of mass m at redshift z, Γ is the number density now (multiplied by any geometrical factor), and $f(m)$ is the normalized mass function. If we ignore any geometrical effects and assume that within each cloud the density and ionization are constant, then the observed H I column density, N, is given by

$$N = Xny , \tag{2}$$

where n is the (hydrogen) number density and X is the hydro-

[3] Due to an error in transcribing the angular diameter–redshift relation, ABC eqs. (2), (3), (6), (10), and (11) are incorrect and should be multiplied by $(1 + z)^2$. In their Fig. 5, all curves should have a slope of 2 added, apart from the one describing the observations. As a consequence, the best fit to the redshift of the numbers of clouds has the H I column density distribution power-law index β in the range 1.75–2.0, and not between 2.0 and 2.25. For a power-law N(H I) distribution, the redshift dependence of the numbers of clouds depends very sensitively on the parameter β. The general conclusion based on their data, that distribution and redshift evolution are consistent with the pressure-confined cloud model, remains true because there are large uncertainties in the value of β.

gen neutral fraction. The cloud mass is

$$m = ny^3 . \tag{3}$$

Thus the observed H I column density is

$$N = Xn^{2/3}m^{1/3} , \tag{4}$$

and equation (1) becomes

$$d\Psi(m, z) = \frac{\Gamma c}{H_0}\left(\frac{m}{n}\right)^{2/3} \frac{(1 + z)}{(1 + 2q_0 z)^{1/2}} f(m)dmdz . \tag{5}$$

If the ionization and density scale as functions of the redshift, as, for example, in the pressure-confined model (ABC), then the cloud mass is measured, to within a redshift-dependent factor, by the column density N. Thus, from equation (4) the column density associated with any feature such as the observed knee in the N(H I) distribution gives a relative value for $Xn^{2/3}$ as a function of redshift. In addition, equation (5) shows that the cross section factor which normalizes the *height* of the N(H I) distribution at each redshift depends only on the cloud density n and a redshift term which depends on the cosmology. Therefore, from the redshift evolution of the N(H I) distribution function we may infer, for a given q_0, the densities and ionization levels in the clouds relative to the values at some redshift. Since the ionization levels are believed to be quite high (Chaffee *et al.* 1986), the ionizing flux $f \propto n/X$, so it is possible to infer relative values for this quantity as a function of redshift as well.

The uncertainties in any determinations we can make for any of these quantities are large, following the discussion of sources of error above, so we are unable to place any strong constraints on the redshift dependence of the cloud properties. Using the value of the shift $\Delta \log N \approx 0.15$, we find that the quantity $Xn^{2/3}$ has increased by a factor of 1.4 as the redshift decreased from $z = 3.5$ to $z = 2.9$, but any value between 0.5 and 4 is acceptable. From the normalization measure above, the quantity $n^{-2/3}[(1 + z)/(1 + 2q_0 z)^{1/2}]$ has reduced to $0.8^{+0.6}_{-0.5}$ times the value at $z = 3.5$ by the time the redshift reaches $z = 2.9$. Thus, for $q_0 = \frac{1}{2}$, the density within the clouds, n, increases with time by a factor $1.2^{+2.8}_{-0.7}$ over this redshift range.

It is of interest to compare these uncertain results with the predictions of the simple model in which the clouds are pressure-confined by a hot adiabatically expanding intergalactic medium. Under these circumstances the cloud temperatures are nearly constant with redshift, or increase slowly as the redshift decreases, and so to maintain pressure balance with the intergalactic medium the density within the clouds should behave as $n \propto (1 + z)^5$ or a higher power. As a consequence, over the range in redshift $z = 3.5$–2.9, the density in the clouds should *decrease* with time by a factor $\gtrsim 2$. Such a decrease is just consistent with the data, but is quite close to the inferred error limit.

Even if it were established that the density within the clouds remains roughly constant over this redshift range it is still possible that the pressure-confined model is consistent with such an observation, provided that the hot intergalactic medium pressure is increasing with time down to redshifts $z \approx 3$. This would be evidence that the intergalactic medium is still being heated at these redshifts. An important test is to establish whether or not there is a dispersion in b values at a given redshift. The simple pressure-confined model allows one temperature at a given redshift, while it is difficult to see how a range of values would not arise if self- (or dark matter) gravity is important. Our data may be consistent with a single velocity dispersion over quite a large range of redshift, but this point requires further investigation.

An alternative possibility is that gravitation plays a role, as discussed by Black (1981) and Melott (1980), or, in a dark matter–dominated model, Rees (1986). The evolution in such cases requires further study.

A second important result follows almost directly from the observations. The Lyα line absorption line density along the spectrum of PKS 2000−330 is approximately constant, with no sign of a turndown in the numbers of clouds near the Lyα emission line until $z \gtrsim 3.74$. At an emission redshift $z = 3.78$, this corresponds to 2500 km s^{-1}. If the true redshift is even higher (work by Gaskell 1982 and Wilkes 1984 suggests adding ~750 km s^{-1} to the redshifts obtained from high ionization emission lines), then the velocity difference will be correspondingly larger. Therefore, at a velocity difference of at least 2500 km s^{-1}, the ionization level in the clouds is not strongly affected by the proximity of the quasar, and so the integrated background ionizing flux must there be at least comparable to that from the quasar. If $m = 17.3$ for PKS 2000−330, for $q_0 = \frac{1}{2}$ we infer that the background ionizing flux at $z = 3.75$ must be of order 3×10^{-21} ergs cm^{-2} s^{-1} Hz^{-1} sr^{-1} or more. This flux is compatible with an extrapolation of the curve given by ABC for a population of quasars with no redshift cutoff. However, it rules out any pronounced cutoff in the numbers of quasars with increasing redshift between $z \approx 2$ and $z \approx 4$, *if* the background quasar population is the dominant source of ionizing photons. An alternative explanation of the required high ionizing flux is that there is some other background source. Recent calculations by D. Tytler (private communication) predict a flux of 2×10^{-21} ergs cm^{-2} s^{-1} Hz^{-1} sr^{-1} from a combined population of quasars with a redshift cutoff at $z = 5$ and early galaxies. Additional calculations by Bechtold *et al.* (1987) also suggest that primeval galaxies may be very important. As far as we know, our observations of PKS 2000−330 offer the best observational constraints to date concerning the possible integrated Lyman-continuum fluxes emitted by these objects.

V. CONCLUSIONS

By combining optical spectra with resolution ≤35 km s^{-1} of three high-redshift quasars, we have been able to examine the redshift evolution of the H I column density and the internal velocity dispersion distributions in intervening absorbing clouds. We find the following:

1. The H I Doppler parameter (b) changes little over the redshift range $1.9 < z < 3.7$, with a mean value of order 30–35 km s^{-1} for well-determined systems with log N(H I) > 13.75. The dispersion in the observed b-distribution is comparable with the mean parameter error for individual measurements, so the data are consistent with many of the clouds having the same internal velocity dispersion. However, the observational uncertainties are sufficiently large that we do not know whether or not a single velocity dispersion applies in nearly all cases.

2. There is an indication that the observed H I column density distribution may not be a single power law as had earlier been supposed, but may flatten toward lower values of N(H I). If the change of slope in the H I column density dis-

tribution is real, and subject to the assumptions that the clouds are uniform and that any redshift-dependent quantities such as ionization or size scale similarly for all clouds, the redshift dependence of the density of material within the clouds may be inferred. On the basis of the available data, it appears that this density increases marginally as the redshift decreases from $z = 3.5$ to $z = 2.9$. However, the data are also consistent with the expectation on a simple pressure-confined cloud model (e.g., Ostriker and Ikeuchi 1983) where the internal density should decrease by a factor of order 2. If the clouds are gravitationally bound, then the observational data suggests that there is no strong redshift evolution either in the densities or Doppler parameters of the material within them.

Out observations of PKS 2000−330 show that the intervening clouds cannot be ionized principally by the integrated light of the background distribution of quasars, *if* that distribution cuts off sharply between $z \approx 2$ and $z \approx 4$. A possible interpretation is that young galaxies provide most of the ionizing flux at high redshifts.

We thank Dr. D. Tytler for his very useful and detailed comments on the manuscript, and also Dr. R. W. Hunstead, Dr. M. Pettini, and Professor J. H. Oort for bringing a number of points to our attention. We are grateful to the CTIO time assignment committee for a generous allocation of telescope time, and to the CTIO mountain staff for their usual excellent assistance with the observing. R. F. C. thanks the Radcliffe Trust for support during the early part of this investigation.

REFERENCES

Atwood, B., Baldwin, J. A., and Carswell, R. F. 1982, *Ap. J.*, **257**, 559.
———. 1985, *Ap. J.*, **292**, 58 (ABC).
Bechtold, J., Weymann, R. J., Malkan, M., and Lin, Z. 1987, *Ap. J.*, **315**, 180.
Black, J. H. 1981, *M.N.R.A.S.*, **197**, 553.
Carswell, R. F., Morton, D. C., Smith, M. G., Stockton, A. N., Turnshek, D. A., and Weymann, R. J. 1984, *Ap. J.*, **278**, 486.
Carswell, R. F., Whelan, J. A. J., Smith, M. G., Boksenberg, A., and Tytler, D. 1982, *M.N.R.A.S.*, **198**, 91.
Chaffee, F. H., Foltz, C. B., Bechtold, J., and Weymann, R. J. 1986, *Ap. J.*, **301**, 116.
Chaffee, F. H., Weymann, R. J., Latham, D. W., and Strittmatter, P. A. 1983, *Ap. J.*, **267**, 12.
Chen, J.-S., Morton, D. C., Peterson, B. A., Wright, A. E., and Jauncey, D. L. 1984, *Proc. Astr. Soc. Australia*, **3**, 355.
Gaskell, C. M. 1982, *Ap. J.*, **263**, 79.
Green, R. F. 1986, in *IAU Symposium 119*, *Quasars*, ed. G. Swarup and V. K. Kapahi (Dordrecht: Reidel), p. 429.
Hunstead, R. W., Murdoch, H. S., Peterson, B. A., Blades, J. C., Jauncey, D. L., Wright, A. E., Pettini, M., and Savage, A. 1986, *Ap. J.*, **305**, 496.
Koo, D. C., Kron, R. G., and Cudworth, K. M. 1986, *Pub. A.S.P.*, in press.
Melott, A. L. 1980, *Ap. J.*, **241**, 889.
Murdoch, H. S., Hunstead, R. W., Pettini, M., and Blades, J. C. 1986, *Ap. J.*, **309**, 19.
Osmer, P. S. 1982, *Ap. J.*, **253**, 28.
Ostriker, J. P., and Ikeuchi, S. 1983, *Ap. J.* (*Letters*), **268**, L63.
Peterson, B. A. 1978, in *IAU Symposium 79*, *The Large Scale Structure of the Universe*, ed. M. S. Longair and J. Einasto (Dordrecht: Reidel), p. 389.
Peterson, B. A., Savage, A., Jauncey, D. L., and Wright, A. E. 1982, *Ap. J.* (*Letters*), **260**, L27.
Rees, M. J. 1986, *M.N.R.A.S.*, **218**, 25P.
Sargent, W. L. W., Young, P. J., Boksenberg, A., and Tytler, D. 1980, *Ap. J. Suppl.*, **42**, 41.
Webb, J. K. 1986, Ph.D. thesis, Cambridge University.
Weymann, R. J., Carswell, R. F., and Smith, M. G. 1981, *Ann. Rev. Astr. Ap.*, **19**, 41.
Wilkes, B. J. 1984, *M.N.R.A.S.*, **207**, 73.
Young, P. J., Sargent, W. L. W., Boksenberg, A., Carswell, R. F., and Whelan, J. A. J. 1979, *Ap. J.*, **229**, 891.

B. Atwood: Cerro Tololo Interamerican Observatory, Casilla 603, La Serena, Chile

J. A. Baldwin: Department of Astronomy, Ohio State University, Columbus, OH 43210

R. F. Carswell: Institute of Astronomy, Madingley Road, Cambridge CB3 0HA, England

J. K. Webb: Sterrewacht Leiden, P.O. Box 9513, 2300 RA Leiden, The Netherlands